Enhancement of Humidity Sensing of PVDF/PEO Nanocomposites Doped with Tungsten Oxide

Aseel N. Bardan
Lamia K. Abbas

Department of Physics, College of Science, University of Baghdad, Baghdad, IRAQ

The study delved into the impact of nano-tungsten oxide doping on PVDF/PEO thin films, meticulously fabricated through the spin coating technique. By modifying the weight percentages of WO_2 nanoparticles (NPs), the study revealed significant findings. X-ray diffraction (XRD) technique provided insight into the polycrystalline nature and tetragonal structure of the films. The morphology of the films was examined using field-emission scanning electron microscopy (FE-SEM), which confirmed the homogenous distribution of WO_2 NPs throughout the PVDF/PEO composite. Further chemical analysis was conducted using Fourier-transform infrared (FTIR) spectroscopy, which identified specific functional groups and elucidated the chemical complexities introduced by the doping material. Optical measurements indicated the energy gap increase from 3.0 eV to 3.2 eV, corresponding with the increase in WO_2 NPs content.

Keywords: Tungsten oxide; Nanoparticles; Polymers; Humidity sensor
Received: 01 October 2023; **Revised:** 13 December 2023; **Accepted:** 20 December 2023

1. Introduction

The performance of chemical and physical sensors has been greatly improved recently for use in everyday life and technology [1]. Continuous humidity monitoring is crucial in several aspects of life. Humidity sensors therefore play a major role in many industries and sectors, including the production of chemicals and food, agriculture, climate management, environmental monitoring, and health, as well as a number of industrial sectors including electronics, paper, automotive, and pharmaceuticals [2]. The creation of high-quality, precise humidity sensors starts with a very low hysteresis, which is followed by a minimal temperature impact, quick recovery times, thermal stability, long-term durability, resistance to pollutants, cheap cost, and a wide range of RH sensitivity [3]. Numerous materials, including ceramics, semiconductors, and polymers, are used to create humidity sensors. These sensors use a variety of mechanisms, such as changes in resistance, capacitance, surface acoustic waves, optical fibers, and quartz crystal microbalance, to measure the humidity level [4]. Capacitive sensors are the most extensively utilized because of their specialized and affordable sensing methods [5].

Lately, doping of nanoparticles, including metal oxides,(CuO, SnO_2, Al_2O_3, ZnO,WO_2), and hydrophilic polymers (PEI , PEO , PVA and PANI) have been utilized as composite sensors to obtain an improved sensitivity and response time [6]. Polyethylene oxide (PEO) is a versatile and harmless polyether, widely utilized in the formulation of pharmaceuticals, food products, and cosmetic items. This polymer has garnered considerable attention for its ability to act as a solid medium for dissolving salts, which is crucial in the development of polymer electrolytes [7]. Moreover, the incorporation of inorganic nanoparticles into polymers, a process known as doping, has expanded the functional range of PEO, making it highly sought after in fields such as catalysis, energy storage [8], electronics, and optoelectronic applications [9]. Polyvinylidene fluoride (PVDF) is an electroactive polymer known for its electroactivity, piezoelectricity, and biocompatibility, making it ideal for sensors, actuators, energy harvesters, and filtration membranes [10].

Tungsten oxide (WO_3) is classified as an n-type semiconductor with a documented band gap ranging from approximately 2.6 to 2.8 eV [11]. Its intrinsic conductivity results from its non-stoichiometric composition, which leads to the formation of a donor level caused by oxygen vacancy defects within the lattice. Due to the various oxidation states of tungsten, such as 2, 3, 4, 5, and 6, the compound can exist in multiple forms. For example, the common forms of tungsten oxides include tungsten (VI) oxide (WO_3, displaying a lemon-yellow appearance) and tungsten (IV) oxide (WO_2, appearing brown and blue) [12]. These electronic properties make tungsten oxides suitable for diverse applications, such as electrochromic devices, photochromic materials, photocatalysts, and gas sensors [13-15]. This research paper explores the effects of incorporating WO_2 nanoparticles into PVDF/PEO films. The study investigates how different ratios of WO_2 influence the structural, morphological, and optical properties of films prepared from these organic materials.

Characterization techniques such as XRD, FTIR, and UV-visible spectrometry were used for analysis. Furthermore, a humidity sensor based on the capacitance/resistive principle was created using this material, and a thorough examination of the sensor's characteristics was carried out.

2. Experimental Part

The study involved the synthesis of a composite material by combining polyvinylidene fluoride (PVDF) with polyethylene oxide (PEO). Using Gel Permeation Chromatography (GPC), PVDF (purchased from Sigma-Aldrich) demonstrated an average molecular weight of approximatly 534,000, indicating the average length of the polymer chains. This polymer was blended with PEO in powder form, supplied by Merck KgAA, based in Darmstadt, Germany, which possessed a density ranging from 1.11 to 1.20 kg/L. The constituents were mixed in a ratio of 3:1, with PVDF constituting the larger fraction at 75%.

The polymers were dissolved in 20 ml of the highly pure Dimethylformamide (DMF) to produce a homogenized mixture. Following that, the resulting solution was kept at 65°C and continuously swirled for over an hour. Next, at doping levels of 5 % and 10 %, tungsten oxide nanoparticles from Sky Spring Nanomaterials, Inc. were added to the solution. These nanoparticles were mixed with the polymer matrix after first dissolving in an extra 20 ml of DMF. To guarantee consistency, the resulting solution was constantly agitated at 65°C for four hours. Following, at a substrate temperature of 65°C, the spin coating procedure produced PVDF/PEO/WO_2 NP hybrid nanocomposite thin films. The samples were expertly dried by spin coating using a Toos Nano Spin Coater (Model SPC-TN-556), and it took one minute for each sample to dry entirely.

The procedure involved depositing the polymer blend on a 2.5×2.5 cm glass substrate and subjecting it to rapid rotation. The spin coating was executed in three stages at different velocities: starting at 5500 rpm for 35 s, followed by 4500 rpm for another 35 s, and concluding at 1000 rpm for 20 s, totaling a 90s duration. This process was instrumental in the solvent's evaporation, resulting in the formation of dry nanocomposite films. The elevated temperature of the substrate during the spin coating was crucial for the swift evaporation and subsequent solidification of the films, thus ensuring their structural and morphological stability. Spin coating at a substrate temperature of 65°C was used effectively to successfully manufacture PVDF/PEO/WO_2 NPs hybrid nanocomposite thin films.

An Analytical X′ Pert Pro X-ray diffraction spectrometer was used to investigate the dried thin films in order to analyze the crystal structure. A JSM-7600 F field-emission scanning electron microscope (FESEM) from Japan's JEOL Ltd. was used to examine the microstructure. The films were covered in a coating of gold before being analyzed. Functional groups and bonds within the samples were identified using a Shimadzu FTIR-1800 spectrometer for Fourier-transform infrared (FTIR) spectroscopy. The manufactured samples were tested for optical energy gap using a Shimadzu UV-visible spectrophotometer (UV160A) at room temperature within the 200-1100 nm wavelength range.

A homemade humidity chamber with a closed chamber, gas inlet, and outlet valves was used to describe the humidity sensor. A combination of moist air and dry nitrogen was used to regulate the humidity levels inside the chamber, enabling a range of humidity ranges from 31 to 100% RH (relative humidity). The GW Instek LCR-821 LCR meters were used to assess the properties of the humidity sensor.

3. Results and discussion

The crystal structure of pure PVDF/PEO films doped with WO_2 with various doping ratios and weight ratios of 75/25 wt.% was studied using an X-ray diffraction spectrometer. The XRD patterns of PVDF/PEO and PVDF/PEO/WO_2 thin films are shown in Fig. (1). Several peaks in the diffraction pattern before and after doping indicate that the produced films are polycrystalline [9]. In the pure sample several peaks were observed at 2θ of 19.1°, 20.2° and 23.4° about the (120), (110) and (010) planes which indicated for PVDF/PEO films [16-18]. After doping, it observed peaks shifted toward higher angle maybe due to the ionic radii value of WO_2 [19]. It was detected the development of other peaks at the angles 25.8°, 36.9°, 37.5°, 52.9°, 53.6°, and 59.8° that belong to the planes (110), (200), (101), (220), (111) and (310), respectively [9].

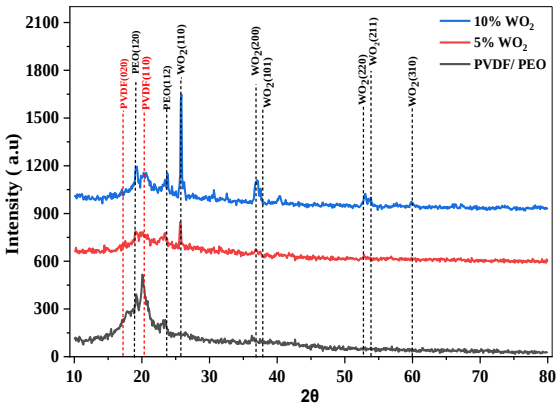

Fig. (1) XRD patterns of PVDF/ PEO and PVDF/PEO/WO_2 thin films at different percentages (5% and 10%) of WO_2

Additionally, the intensity of these new peaks increases as the fraction of WO_2 particles increases, providing evidence of improved crystal structure [20]. The peaks' sharpness indicates the great crystallinity that was attained. The average crystal size (D) was estimated using Scherer's formula [21].

$$D = \frac{k\lambda}{\beta \cos\theta} \quad (1)$$

where D is crystallite size, k (=0.94) is shape factor, λ (=0.154 nm) is the wavelength of radiation, β is the full width half maximum and θ is the position of the peak. The average crystal size (D) was found to be 14.3, 14.76 and 19.4 nm for pure, 5% and 10% WO_2, respectively. When the WO_2 content is increased, the average crystallite size increased. This could be because the crystal coarsened and the Ostwald ripening mechanism caused the growth [22].

It was observed that its intensity increased with increasing the doping ratios, and an improvement in the structural properties of the prepared films was also observed as a result of the increase in the average size of the crystals [23].

This work used SEM at multiple scales and magnification levels to explore how doping WO_2 at different weight ratios affected PVDF/PEO (75/25 wt.%) films' surface properties. Figure (2a) demonstrates the presence of hexagonal-like α-phase PVDF crystals, while PVDF crystals display a fibrous texture similar to tiny fibers [23,24]. The viscosity of PEO appears to be substantial in pure PVDF/PEO hybrid micrographs. These findings are comparable to those of earlier research [25].

Including WO_2 nanoparticles leads to an enhancement in hydrophilicity due to increased porosity, accompanied by numerous spherical nanoparticles and rough surface formation. This figure portrays the effect of incorporating WO_2 nanoparticles into the PVDF/PEO combination. Figures (2b) and (2c) exhibit the images of PVDF/PEO+5% WO_2 nanoparticles and PVDF/PEO+10% WO_2 nanoparticles, respectively, revealing an augmentation in pore size with an increasing weight ratio of WO_2 nanoparticles. When depositing thin films onto substrates, the temperature has crucial effects, in the substrate's glass transition temperature (T_g). When temperature reach near or above the T_g can enhance the mobility of polymer chains, affecting the film's adhesion and morphology.

Using energy-dispersive x-ray spectroscopy (EDX), researchers analyzed the nanocomposites made of PVDF/PEO and PVDF/PEO/WO_2 to determine their precise chemical makeup. Figure (3) illustrates the EDX spectra of PVDF/PEO, PVDF/PEO+5% WO_2 nanoparticles, and PVDF/PEO+10% WO_2 nanoparticles, respectively. The EDX spectrum confirms the presence of WO_2 nanoparticles in the PVDF/PEO composite. The EDX spectrum reveals the presence of carbon as well as tungsten oxide. Carbon and oxide were shown to be the ingredients responsible for forming the PVDF/PEO structure, whereas tungsten (W) and oxide (O) were found to be responsible for forming the WO_2 structure [9].

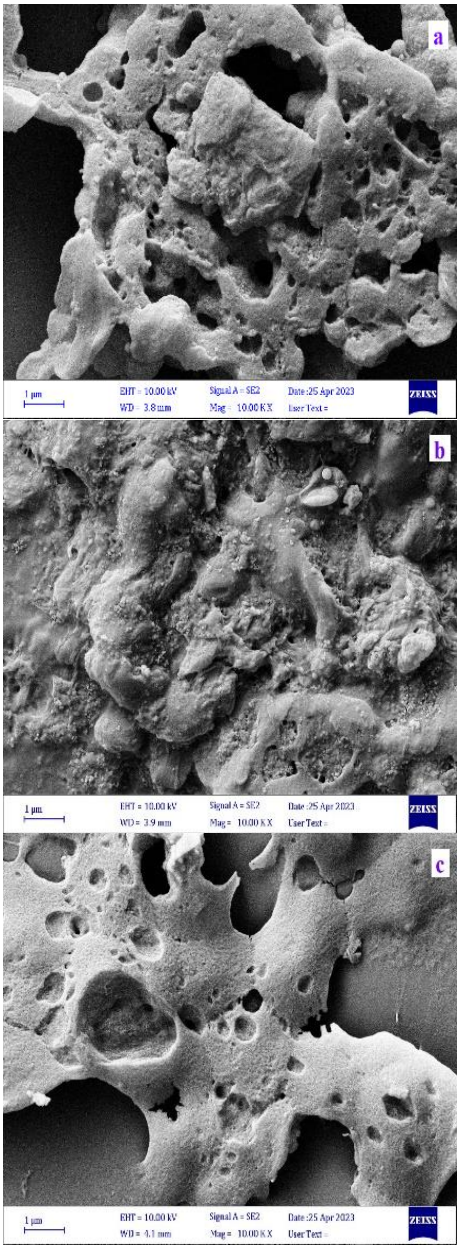

Fig. (2) FE-SEM images of PVDF/PEO and PVDF/PEO/WO_2 (a) pure, (b) 5% WO_2, (c) 10% WO_2

By using their distinctive infrared radiation absorption in vibrational modes, Fourier-transform infrared (FTIR) spectroscopy is a valuable method for identifying chemical bond functional groups [26]. Figure (4) shows the FTIR spectra of PVDF/PEO and (PVDF/PEO)/WO_2 nanocomposite thin films containing 5% and 10%, respectively, of WO_2 NPs as functions of the wavenumber in 960 and 842 cm^{-1}. PVDF bands cover the spectra of the nanocomposites (PVDF/PEO)/WO_2 and (PVDF/PEO)/PEO. Based on the information provided in Fig. (4), PVDF has three distinct polymorph phases, each characterized by a unique set of bands. The presence of WO_2 NPs is confirmed by a band observed at 601 cm^{-1}, which corresponds to the W-O stretching vibration. However, this specific band is not present in the spectra of PVDF/PEO [27]. In both the PVDF/PEO

and (PVDF/PEO)/WO_2 nanocomposites, the crystalline α-phase of PVDF is identified by a specific band within the 840-879 cm^{-1} range, while a band represents the crystalline β-phase at around 879.2 cm^{-1} [28-30]. Additionally, the peak at 1650.54 cm^{-1}, corresponding to the carbonyl group (C-O), is observed, a characteristic feature of PEO. Another band at 1186 cm^{-1} is present, indicating the stretching vibration of surface hydroxyl groups or adsorbed water, possibly due to water re-adsorption from the surrounding atmosphere. The bands at 1436.14 cm^{-1} and 1290.16 cm^{-1}, corresponding to the tungsten-hydroxyl (W-OH) vibrations, are attributed to hydroxyl groups (C-H) [31].

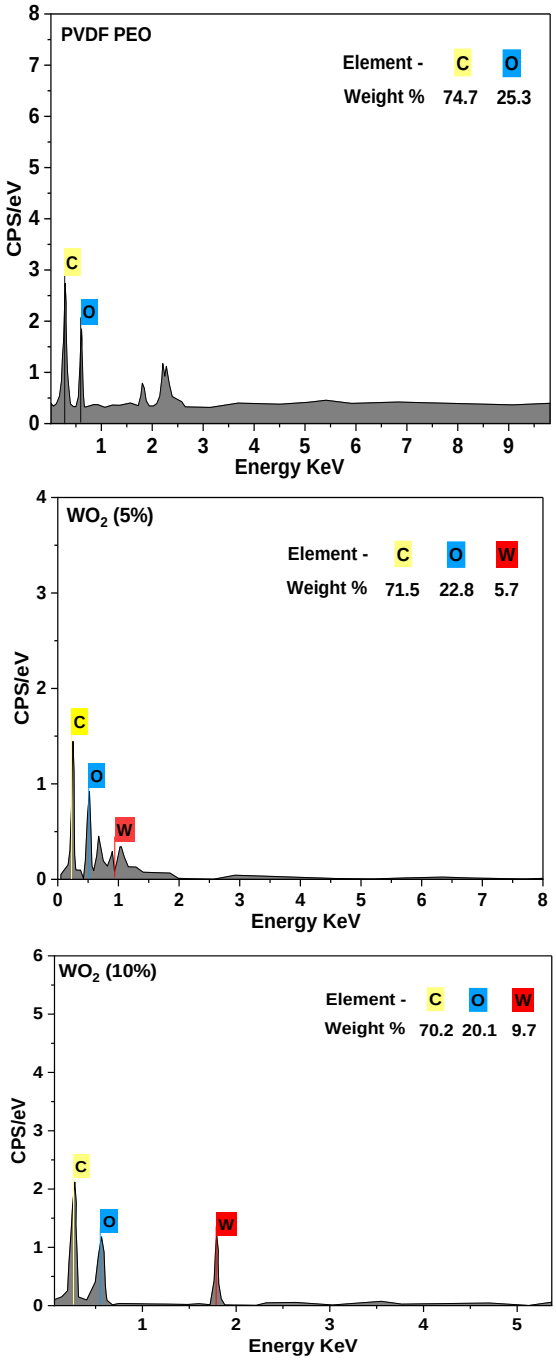

Fig. (3) EDX spectra of a PVDF/PEO and PVDF/PEO/WO_2 at different percentages (5% and 10%) of WO_2 NPs

The transmittance spectrum of nanocomposite thin films, specifically PVDF/PEO and (PVDF/PEO)/WO_2, is presented in Fig. (5). It is evident from the figure that as the weight ratio of WO_2 NPs increases, the transmittance values also rise. At ambient temperature, PVDF/PEO and PVDF/PEO/WO_2 NPs composite thin films were subjected to UV-visible spectroscopy to evaluate their optical characteristics. The wavelength range for this examination ranged from 200 to 1100 nm.

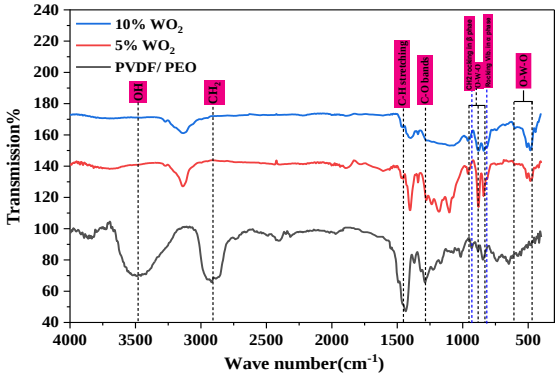

Fig. (4) FTIR spectra of PVDF/PEO and (PVDF/PEO)/WO_2 nanocomposite thin films at ambient conditions

Figure (5) displays the UV-Vis transmittance spectra of PVDF/PEO and PVDF/PEO/WO_2 composite thin films with varying weight ratios of WO_2 NPs (5% and 10% wt.%). The figure demonstrates that transmittance values increase with increasing concentration of WO_2 NPs. In the transmittance spectrum of the PVDF/PEO thin film, the visible region exhibits a transmittance of approximately 33%. However, upon adding 5 and 10 wt.% of WO_2 NPs to the PVDF/PEO combination, the transmittance values rise to 42% and 51.9%, respectively. This increase is illustrated in Fig. (5).

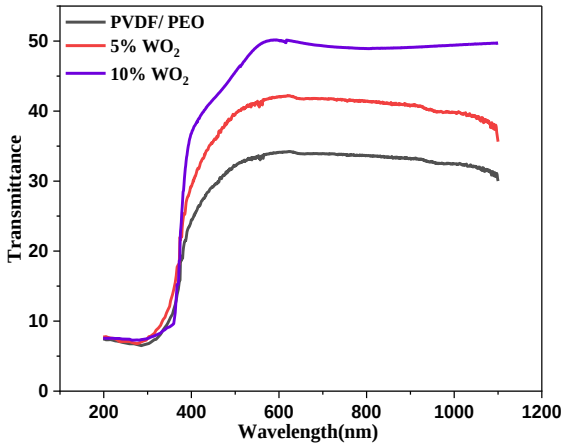

Fig. (5) Transmittance spectra of PVDF/PEO//WO_2 NPs composite thin films with different weight ratios of WO_2 NPs

When taken as a whole, the transmittance spectra of PVDF/PEO/WO_2 nanocomposite thin films point to an increase in permeability in correlation with an increase in the weight ratio of WO_2 NPs. The light scattering mechanism may be less noticeable if WO_2 particles diffuse throughout the polymer chains. This would have the effect of lowering the density as well as the molecular weight. This could explain the observed decrease in surface roughness after doping with WO_2 NPs at varying weight ratios [32,33]. Notably, PVDF/PEO/WO_2 thin films with 5 and 10 wt.% of WO_2 NPs exhibit higher transmittance values. Furthermore, the transmittance of thin films composed of the PVDF/PEO/WO_2 nanocomposite displays a significant decrease in the UV region, which can be attributed to electronic transitions within the band gap.

The values of optical energy gap (E_g) of nanocomposite thin films, namely PVDF/PEO and PVDF/PEO/WO_2 NPs, were determined using the Tauc's equation, which enables the calculation of E_g by analyzing the high absorption area near the absorption edge of these films, as shown in Eq. (2) [34]:

$$\alpha h\nu = B(h\nu - E_g)^r \quad (2)$$

The determination of the optical absorption coefficient (α) involves several factors, including the optical energy gap (E_g), incident photon energy ($h\nu$) in eV, material structure (β), and the index (r) describing the optical absorption process, as described by the provided equation [35,36]. A linear dependence is observed in this relationship, indicating allowed direct transitions. Consequently, the value of E_g is determined by extrapolating the fraction at $\alpha = 0$, as depicted in Figure 6, which shows the Tauc's plot for pure PVDF/PEO. The plot illustrates the dissimilarity of $(\alpha h\nu)^2$ as a function of ($h\nu$) for thin films of PVDF/PEO/WO_2 NPs nanocomposites with different weight ratios (5 and 10 wt.%) of WO_2 NPs. The optical energy gap value of PVDF/PEO is observed to be 3.0 eV. When adding 5 wt.% and 10 wt.% of WO_2 NPs to PVDF/PEO, the optical energy gap values of the resulting films were 3.086 and 3.22 eV, respectively, as shown in Fig. (6).

Increasing the weight ratio of WO_2 NPs leads to an increase in the optical energy gap of PVDF/composite films. Previous studies have indicated that the interaction between WO_2 NPs and the polymer matrix may introduce structural defects and microstrains, which are associated with an increase in the optical energy gap values of PVDF/PEO [37]. Disordered defects and small stresses contribute to the growth of the density of localized states within the band gap [38]. While, Alghamdi et al [39] which loaded the content of single walled carbon nanotubes (SWCNTs) with PVDF/PEO, show that the energy gap reduces as SWCNT load increases because the density of defect states increases.

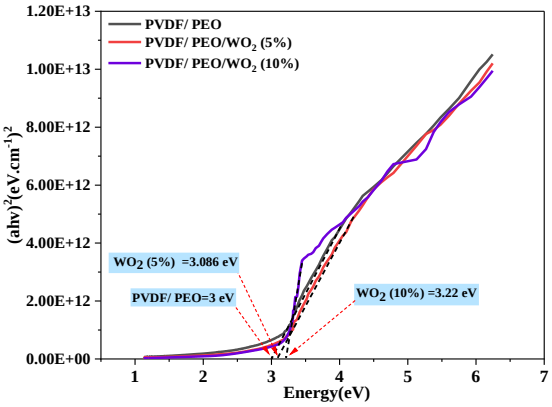

Fig. (6) Tauc's plots for pure PVDF/PEO and PVDF/PEO/WO_2 NPs nanocomposites thin films with different weight ratios (5 and 10 wt.%) of WO_2 NPs

The electrical responses of the humidity sensors were studied on pure PVDF/PEO films and films incorporating tungsten oxide nanoparticles at different weight ratios (5 wt.% and 10 wt.%). These responses were recorded at room temperature to understand the effects of humidity on these films. In the humidity range of 30-100% relative humidity, a specific voltage was applied across the ohmic contact to measure the electrical resistance of the circuit. Figure (7) illustrates the normalized resistance as a function of relative humidity (RH%) for pure PVDF/PEO surface-type humidity sensors doped with WO_2 NPs. The measurements were taken at frequencies of 0.1, 10, 100, 1000, and 2000 kHz. The researchers achieved precise results by applying a specific voltage and measuring the electrical resistance within the humidity range of 30-100 RH%. In the case of the pure PVDF/PEO film, the resistance gradually decreased as RH values increased within the range of 75-100% RH. On the contrary, PVDF/PEO/WO_2 NPs films with 5 and 10 wt.% exhibited a sharp increase in resistance with rising RH% values within the ranges of 65-100% RH and 60-100% RH, respectively. Consequently, higher relative humidity levels led to decreased conductivity. The improved conductivity of PVDF/PEO/WO_2 thin films at higher relative humidity levels can be attributed to several factors. Firstly, the enhanced electronic and ionic conductivity of the films can be linked to their improved dielectric constant. Notably, the ionic conductivity values were strongly correlated with the dielectric constant of the thin film material. The introduction of water into PVDF/PEO/WO_2 NPs thin films augmented their dielectric constant, thereby elevating their ionic conductivity. Secondly, the interaction between PVDF/PEO/WO_2 and water molecules may have dissociated water molecules into ions, further contributing to the films' conductivity.

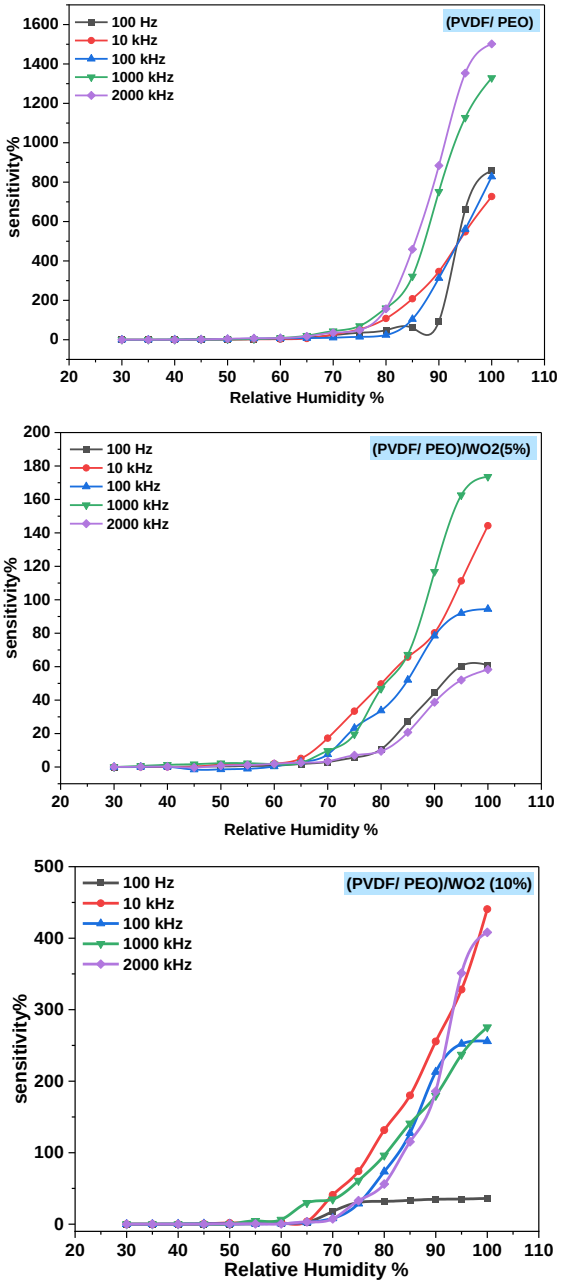

Fig. (7) Normalized resistance as a relative humidity (RH%) function for the surface-type humidity sensor of pure and doped PVDF/PEO with WO_2 NPs with different weight ratios (5 and 10 wt.%)

Figure (7) indicated that all the fabricated films exhibited positive sensitivity at various relative humidity levels. However, it was observed that the sensitivity of the samples treated with tungsten oxide nanoparticles had decreased. Figure (8) shows the normalized capacitance (C) of the surface-type humidity sensor composed of PVDF/PEO/WO_2 NPs, plotted against relative humidity (RH%). Similar to the normalized resistivity measurements, the normalized capacitance and its variation regarding relative humidity exhibit similar behaviour. It was observed that the capacitance decreases as relative humidity increases. Conversely, the sensitivity of the sensor increases with rising relative humidity. Moreover, it was observed that increasing the frequency value leads to higher capacitance values in both pure PVDF/PEO films and doped with WO_2 NPs.

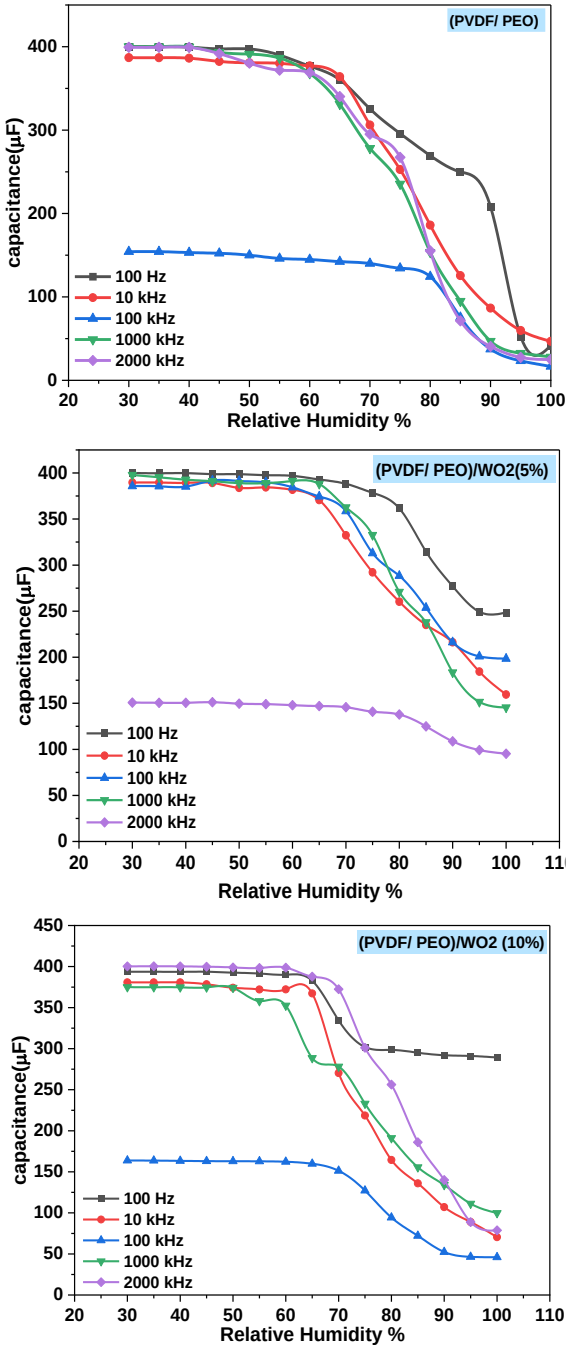

Fig. (8) Normalized capacitance sensitivity (SC) versus the relative humidity for pure and doped PVDF/PEO with WO_2 NPs with different weight ratios (5 and 10 wt.%)

4. Conclusion

Incorporating tungsten oxide nanoparticles into PVDF/PEO nanocomposite films resulted in a substantial alteration of the characteristics of the films. The films were found to have a polycrystalline structure and the presence of hexagonal-like-phase PVDF crystals was confirmed, whereas the PVDF

crystals had a fibrous texture comparable to the texture of tiny fibres. The presence of carbon and oxide coming from the PVDF/PEO structure was verified. The optical energy gap of PVDF/PEO increased from 3.0 to 3.2 eV with incrementing the WO_2 NPs weight ratio. It was observed that all the prepared films showed positive sensitivity at different levels of relative humidity. However, it should be noted that the sensitivity of samples treated with WO_2 NPs decreased and that the best sensitive samples were the uninoculated samples.

References

[1] G. Shah et al., "Resistive-and capacitive-type humidity and temperature sensors based on a novel caged nickel sulfide for environmental monitoring", *J. Mater. Sci. Mater. Electron.*, 31 (2020) 3557-3563.

[2] B. Cai et al., "Semiconducting single-walled carbon nanotube/graphene van der Waals junctions for highly sensitive all-carbon hybrid humidity sensors", *J. Mater. Chem. C*, 8(10) (2020) 3386-3394.

[3] S. Kundu et al., "Relative humidity sensing properties of doped polyaniline-encased multiwall carbon nanotubes: Wearable and flexible human respiration monitoring application", *J. Mater. Sci.*, 55(9) (2020) 3884-3901.

[4] Z. Chen and C. Lu, "Humidity sensors: a review of materials and mechanisms", *Sens. Lett.*, 3(4) (2005) 274-295.

[5] M. Sajid et al., "Liquid-assisted exfoliation of 2D hBN flakes and their dispersion in PEO to fabricate highly specific and stable linear humidity sensors", *J. Mater. Chem. C*, 6(6) (2018) 1421-1432.

[6] W. Ahmad et al., "Highly sensitive humidity sensors based on polyethylene oxide/CuO/multi walled carbon nanotubes composite nanofibers", *Materials (Basel)*, 14(4) (2021) 1037.

[7] V. Caramia et al., "Tailoring the morphology of poly (ethylene oxide)/silver triflate blends: from crystalline to self-assembled nanofibrillar structures", *Nanotechnol.*, 24(5) (2013) 55602.

[8] C. Pittarate et al., "Effects of poly (ethylene oxide) and ZnO nanoparticles on the morphology, tensile and thermal properties of cellulose acetate nanocomposite fibrous film", *Polym. J.*, 43(12) (2011) 978-986.

[9] A.K. Khaleel and L.K. Abbas, "Synthesis and characterization of PVDF/PMMA/ZnO hybrid nanocomposite thin films for humidity sensor application", *Optik*, 272 (2023) 170288.

[10] S. Barrau et al., "Nanoscale investigations of α- and γ-crystal phases in PVDF-based nanocomposites", *ACS Appl. Mater. Interfaces*, 10(15) (2018) 13092-13099.

[11] M.A. Butler, "Photoelectrolysis and physical properties of the semiconducting electrode WO_2", *J. Appl. Phys.*, 48(5) (1977) 1914-1920.

[12] S. Supothina et al., "Synthesis of tungsten oxide nanoparticles by acid precipitation method", *Ceram. Int.*, 33(6) (2007) 931-936.

[13] M. Sun et al., "Nanocrystalline tungsten oxide thin film: preparation, microstructure, and photochromic behavior", *J. Mater. Res.*, 15(4) (2000) 927-933.

[14] C.G. Granqvist, "Electrochromic tungsten oxide films: review of progress 1993-1998", *Sol. Energy Mater. Sol. Cells*, 60(3) (2000) 201-262.

[15] G.R. Bamwenda and H. Arakawa, "The visible light induced photocatalytic activity of tungsten trioxide powders", *Appl. Catal. A Gen.*, 210(1-2) (2001) 181-191.

[16] R.S. Hafez et al., "Dielectric and thermal properties of PEO/PVDF blend doped with different concentrations of $Li_4Ti_5O_{12}$ nanoparticles", *J. Inorg. Organomet. Polym. Mater.*, 30 (2020) 4468-4480.

[17] L. Sannier et al., "Lithium metal batteries operating at room temperature based on different PEO-PVdF separator configurations", *J. Electrochem. Soc.*, 151(6) (2004) A873.

[18] Q. Ye et al., "Fabricating a PVDF skin for PEO-based SPE to stabilize the interface both at cathode and anode for Li-ion batteries", *J. Energy Chem.*, 70 (2022) 356-362.

[19] M. Ginting et al., "Preparation and characterization of zinc oxide doped with ferrite and chromium", in *AIP Conf. Proc.*, 1862(1) (2017).

[20] S.H. Mujawar et al., "Electrochromic properties of spray-deposited niobium oxide thin films", *Solid State Ionics*, 177(37-38) (2006) 3333-3338.

[21] S.M.H. Al-Jawad et al., "Influence of nickel doping concentration on the characteristics of nanostructure CuS prepared by hydrothermal method for antibacterial activity", *Surf. Rev. Lett.*, 28(01) (2021) 2050031.

[22] S. Suwanboon and P. Amornpitoksuk, "Preparation of Mg-doped ZnO nanoparticles by mechanical milling and their optical properties", *Procedia Eng.*, 32 (2012) 821-826.

[23] T. Iqbal et al., "Investigations on ZnO/polymer nanocomposite thin film for polymer based devices", *Mater. Res. Exp.*, 6(7) (2019) 75322.

[24] C. Rameshkumar et al., "Preparation and characterization of pristine PMMA and PVDF thin film using solution casting process for optoelectronic devices", *J. Surf. Sci. Technol.*, 33 (2017) 12-18.

[25] P. Dhatarwal and R.J. Sengwa, "Impact of PVDF/PEO blend composition on the β-phase crystallization and dielectric properties of silica nanoparticles incorporated polymer nanocomposites", *J. Polym. Res.*, 26(8) (2019) 196.

[26] H. Wang et al., "Comparison of conductometric humidity-sensing polymers", *Sens. Actuat. B*

Chem., 40(2-3) (1997) 211-216.
[27] S.M. Costa et al., "Multifunctional flax fibres based on the combined effect of silver and zinc oxide (Ag/ZnO) nanostructures", *Nanomaterials*, 8(12) (2018) 1069.
[28] X. Cai et al., "A critical analysis of the α, β and γ phases in poly(vinylidene fluoride) using FTIR", *RSC Adv.*, 7(25) (2017) 15382-15389.
[29] P. Martins, A.C. Lopes and S. Lanceros-Mendez, "Electroactive phases of poly (vinylidene fluoride): Determination, processing and applications", *Prog. Polym. Sci.*, 39(4) (2014) 683-706.
[30] Z. Cui et al., "Crystalline polymorphism in poly (vinylidenefluoride) membranes", *Prog. Polym. Sci.*, 51 (2015) 94-126.
[31] F.F. Gondim et al., "Poly (vinylidene fluoride) with zinc oxide and carbon nanotubes applied to pressure sheath layers in oil and gas pipelines", *J. Appl. Polym. Sci.*, 138(14) (2021) 50157.
[32] A.P. Indolia and M.S. Gaur, "Optical properties of solution grown PVDF-ZnO nanocomposite thin films", *J. Polym. Res.*, 20 (2013) 1-8.
[33] M.I. Mohammed, "Optical properties of ZnO nanoparticles dispersed in PMMA/PVDF blend", *J. Mol. Struct.*, 1169 (2018) 9-17.
[34] J. Tauc and A. Menth, "States in the gap", *J. Non. Cryst. Solids*, 8 (1972) 569-585.
[35] Z. Li and C. Wang, **"One-dimensional Nanostructures: Electrospinning Technique and Unique Nanofibers**", Springer (2013).
[36] C.J. Thompson et al., "Effects of parameters on nanofiber diameter determined from electrospinning model", *Polymer (Guildf).*, 48(23) (2007) 6913-6922.
[37] S. Pervaiz et al., "Study of structural, optical and dielectric properties of ZnO/PVDF-based flexible sheets", *J. Polym. Res.*, 28 (2021) 1-13.
[38] S. Shukla, N.K. Sharma and V. Sajal, "Theoretical analysis of surface plasmon resonance based fiber optic sensor using ITO and ZnO thin films", *Opt. Quantum Electron.*, 48 (2016) 1-9.
[39] H.M. Alhusiki-Alghamdi and N.S. Alghunaim, "Spectroscopic studies of nanocomposites based on PEO/PVDF blend loaded by SWCNTs", *J. Mod. Phys.*, 6(04) (2015) 414.

